Available online at www.sciencedirect.com
SCIENCE DIRECT®
Coordination Chemistry Reviews 249 (2005) 1382–1395
COORDINATION CHEMISTRY REVIEWS
www.elsevier.com/locate/ccr

Review

Photochemical reactions leading to NO and NO_x generation

Peter. C. Ford*, Stephen Wecksler

Department of Chemistry and Biochemistry, University of California, Santa Barbara, CA 93106-9510, USA

Received 5 August 2004; accepted 26 October 2004
Available online 16 December 2004

Contents

Abstract

Studies in this laboratory are concerned with elucidating chemical mechanisms relevant to roles played by nitrogen monoxide and other NO_x species in mammalian bioregulation and immunology. Dynamic photochemical techniques have proved very useful in probing these mechanisms. We also have interest in strategies to deliver NO to biological targets upon demand for such goals as the sensitization of γ-radiation damage in hypoxic tissue. One such strategy would be to employ a precursor that displays relatively low thermal reactivity but is photochemically active to release NO. This proposition has led us to investigate the flash and continuous photolysis kinetics of a number of different nitrosyl complexes and other NO and NO_x precursors such as metal nitrito complexes. The systems probed include several ruthenium salen and porphyrin nitrosyls, manganese(III) and chromium(III) nitrito complexes, ferri- and ferro-heme models and proteins, and iron-sulfur-nitrosyl clusters known as the Roussin's anions (e.g. $Fe_2S_2(NO)_4^{2-}$) and esters (e.g., $Fe_2(\mu\text{-}SR)_2(NO)_4$, where R is an organic functional group). An overview of these studies is presented.

Keywords: Photochemistry; Nitric oxide; Transition metal; Metal nitrosyls; Porphyrins; Salens; Chromium/manganese nitrito complexes; Cyclams; Iron sulfur nitrosyls; Two photon excitation

1. Introduction

In the early 1990s, we initiated studies at UCSB and collaboratively with Mikio Hoshino and coworkers at RIKEN (Japan) into the photochemical reactions of metal nitrosyl complexes [1]. These projects were stimulated by discussions with Drs. Larry Keefer and David Wink at the National Cancer Institute regarding the biological roles of nitric oxide (nitrogen monoxide). They drew our attention to the (then) recent discoveries that NO is an intercellular bioregulatory agent in mammalian cardiovascular and nervous systems and

* Corresponding author. Tel.: +1 805 893 2443; fax: +1 805 893 4120.
E-mail address: ford@chem.ucsb.edu (Peter.C. Ford).

0010-8545/$ – see front matter © 2004 Elsevier B.V. All rights reserved.
doi:10.1016/j.ccr.2004.10.022

is also a toxic species formed by macrophages in immune response to pathogens [2–6]. Furthermore, key targets of NO reactivity in bioregulatory roles involve coordination complexes. These discoveries as well as the apparent relationship of over- or under-production of NO to various disease states has led to an outpouring of contributions to the chemical, biological and biomedical literature. Despite this activity, fundamental issues regarding the condensed phase chemistry of NO and related species such as nitrogen dioxide (NO_2), peroxynitrite ($OONO^-$) and hydrogen nitrosyl (HNO) need further analysis. For example, although metals are primary targets in the biological chemistry of NO, until recently little attention had been given to the mechanisms for the formation of metal–NO bonds.

Since the initial studies with Hoshino et al. [1] and Wink et al. [7], our involvement has grown into major research effort at UCSB concerned with exploring photochemical strategies for the delivery of NO to biological targets and with the use of kinetic flash photolysis techniques in mechanistic investigations of related NO thermal reactions. Here we present an overview of several related investigations concerned with the quantitative photochemistry of metal complexes.

Why photochemical delivery of NO to targeted tissues? Controlled release of NO at specific physiological sites has both known and potential biomedical applications. For example, nitroglycerine and sodium nitroprusside were used as vasodilator agents long before the discovery that NO is produced endogenously. Another potential application would be the sensitization of γ-radiation damage in hypoxic tumor cells. Normal cells are often more susceptible to radiation than are tumor cells owing to the higher oxygen tension in the former. As a consequence, a desirable goal is to increase the effectiveness of radiation treatment in the latter by using sensitizers to enhance the cell-killing impact of specific doses. NO has long been known to be such a sensitizer [8,9]; however, administering a thermal NO donor would be challenged by the need to target specific cells and by the cardiovascular and other implications of systemic application. On the other hand, if a thermally stable compound were given to the host that could be triggered to release NO in a spatially confined manner, then it would be possible to enhance sensitivity of the targets while not affecting other tissues. Metal nitrosyls, for example, are potential NO carriers that can be triggered by illumination with light of the appropriate wavelength with specific targeting through control of irradiation areas and intensities. It is also of interest to design compounds that have absorbtivity and photoreactivity at wavelengths where light transmission through tissue is optimal. Much of the research described here was initiated in the context of such a goal.

Scheme 1 illustrates different strategies for NO photoproduction currently under study in this laboratory. The first two involve metal nitrosyl complexes, and there is a rich history of nitrosyl complex photochemistry, especially that involving metalloporphyrins [3]. The third (the "indirect method") generates NO not by labilization of an M–NO bond but from homolysis of an O–N bond of coordinated nitrite. Discussed in the sections below are examples from each of these approaches and the latter part of the review focuses on recent studies with the Roussin's salt anions and esters, which are iron/sulfur/nitrosyl clusters. For one of the esters, two photon excitation has proved to be an alternative strategy for NO photo-generation utilizing near-infrared excitation wavelengths.

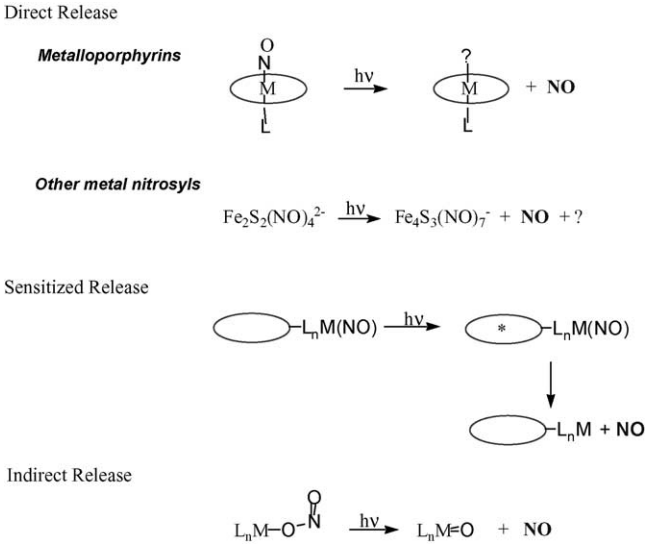

Scheme 1. Photochemical strategies for NO delivery.

As noted above, another on-going goal is to elucidate key reactions of NO and related NO_x species with biologically relevant substrates. While many of these studies can be initiated by standard thermal reaction techniques, others, especially reactions with highly labile metal centers require fast reaction methodologies. In this context, we have also utilized time-resolved spectroscopic techniques to probe the rates and mechanisms of NO and NO_x reactions with model heme compounds, several ferriheme proteins and various ruthenium complexes using laser flash photolysis.

2. Photoreactions of ruthenium porphyrin and ruthenium salen nitrosyl complexes

Thermal stability is a necessary characteristic for a photoactive NO carrier. It was this feature that turned our attention to the ruthenium complexes, since Ru-nitrosyls are generally quite robust. Another desirable characteristic for photochemical bio-activity is red-light sensitivity owing to the greater penetration of red light into tissue [10]. It was with these considerations that we began to explore the photochemistry of ruthenium porphyrin nitrosyl complexes (Ru(P)(X)(NO), e.g., P = TPP (tetraphenylporphyrin) or OEP (octaethylporphyrin)), since porphyrins have strong absorptions in the red. These were first prepared by the reaction

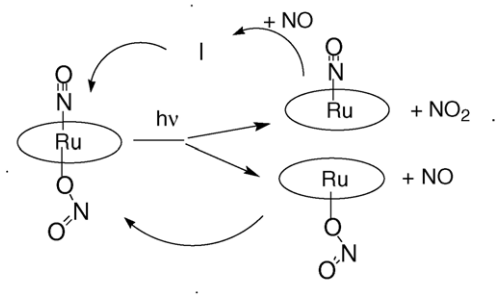

Scheme 2. Transients formed by laser flash photolysis of Ru(P)(NO(ONO)) in benzen.

shown in Eq. (1) [11,12]:

$$Ru(P)(CO) + 4NO \rightarrow Ru(P)(NO)(ONO) + CO + N_2O \quad (1)$$

The various Ru(P)(NO)(X) displayed a rich photochemistry owing to competitive excited state reactions [13]. For example, flash photolysis studies of Ru(TPP)(NO)(ONO) in hydrocarbon solvents demonstrated that two short-lived intermediates are formed. The decay kinetics clearly demonstrated that the temporal absorbance could be best fit to two [NO] dependent exponentials. One of these processes is reversible NO photolabilization to give the Ru(III) intermediate Ru(TPP)(ONO), which displays a fast second order back reaction with NO with a k_{NO} of $2.8 \times 10^8\ M^{-1}\ s^{-1}$. The other involves NO_2 dissociation to give the transient species Ru(TPP)(NO). Similar nitrogen dioxide release is also a photoreaction of the manganese nitrito complex Mn(TPP)(ONO) described below [14]. That NO_2 dissociation is seen indicates the electronic flexibility of the Ru(P)(NO) chromophore, since this (formally) involves reduction of a $\{MNO\}^6$ to a $\{MNO\}^7$ system [15]. The regeneration of the starting nitrosyl nitrito species is a complicated transformation, involving formation of a dinitrosyl complex Ru(TPP)$(NO)_2$ (I) via a second order reaction of Ru(TPP)NO with NO ($2 \times 10^7\ M^{-1}\ s^{-1}$) followed by further reaction with NO to give Ru(TPP)(NO)(ONO) plus N_2O in analogy to Eq. (1) [16] (Scheme 2)

Another synthetic platform for ruthenium NO carriers is based on the salen-type complexes Ru(R-salen)(X)(NO), (salen = *N*,*N*′-bis(salicylidene)-ethylenediaminato dianion) and related salophen complexes Ru(R-salophen)(X)(NO) (salophen = *N*,*N*′-1.2-phenylenediamine-salicylideneiminato dianion). Additional interest in these derives from demonstrations that Ru(R-salen)(X)(NO) compounds are photochemically activated catalyst precursors for alkene asymmetric epoxidations and cyclopropanations and asymmetric hetero Diels–Alder reactions [17]. Flexibility is provided by modifying substituents on the salen and salophen ligands to prepare a series of compounds where systematic variations lead to predictable differences in the absorption spectra, solubilities and photochemical reactivities.

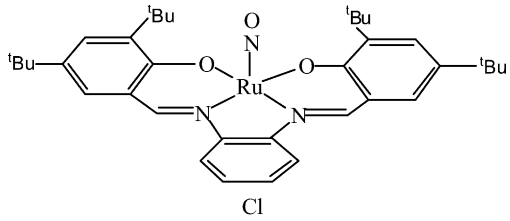

Ru((tBu)$_4$salophen)(Cl)(NO)

We have carried out photoreactivity investigations on a representative members of this family (for example, Ru(salen)(Cl)(NO)) in various media [18,19]. These demonstrate that NO is labilized to give solvento Ru(III) complexes (Eq. (2)) of the type that are the likely active species in the photochemically generated catalysts referenced above. Quantum yields for 365 nm irradiation in acetonitrile solution fall in a fairly narrow range (0.06–0.13) but decrease at longer λ_{irr}. The thermal reverse reaction to regenerate Ru(salen)(Cl)(NO) is strongly dependent on the nature of the solvent Sol, with second order rate constants k_{NO} (298 K) ranging ~11 orders of magnitude, from $4 \times 10^7\ M^{-1}\ s^{-1}$ in toluene to $\sim 5 \times 10^{-4}\ M^{-1}\ s^{-1}$ in acetonitrile [19]. This suggests that the back reaction proceeds via a dissociative mechanism, the rate of Ru–NO bond formation controlled by the lability of Sol. The results of activation parameter studies are consistent with this interpretation. When Ru(tBu$_4$salen)(Cl)(NO) (tBu$_4$salen = *N*,*N*′-ethylene-bis(3,5-di-*t*-butly-salicylideneiminato) dianion) in toluene solution was subjected to flash photolysis, temperature effects on the back reaction rates gave $\Delta H^{\ddagger}_{NO} = 34 \pm 2\ kJ\ mol^{-1}$ and $\Delta S^{\ddagger}_{NO} = +10 \pm 6\ J\ mol^{-1}\ K^{-1}$ while hydrostatic pressure effects gave $\Delta V^{\ddagger}_{NO} = +22 \pm 2\ cm^3\ mol^{-1}$.

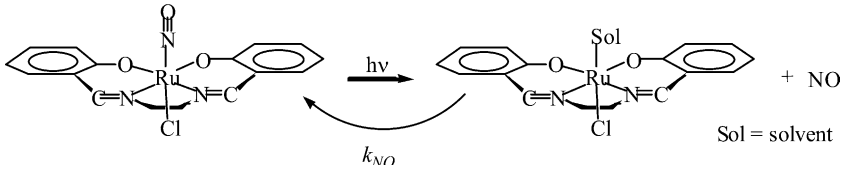

(2)

Notably, flash photolysis of the nitrito nitrosyl complex Ru(salen)(NO)(ONO) led to formation of a single intermediate, Ru(salen)(ONO)(Sol) (Sol = solvent) generated by NO loss [30]. This contrasts to the porphyrin analogs Ru(P)(ONO)(NO) that undergo competitive loss of NO *and* NO_2 as illustrated in Scheme 2. In preliminary studies, we have also prepared the ionic complex $[Ru(salen)(H_2O)(NO)]^+$ and demonstrated photochemistry in aqueous solution analogous to that of Ru(salen)(Cl)(NO) [19]. The thermal stability of ruthenium nitrosyl complexes has drawn the attention of other researchers [20], who have

reported the photolabilization of NO from a variety of such compounds including studies of analogous ruthenium salen complexes by Bordini et al. [20a].

3. Flash photolysis studies of ferri- and ferro-heme models and proteins

The best defined target for NO in bioregulatory action is the ferroheme enzyme soluble guanylyl cyclase (sGC). The formation of a Fe(II)–NO complex leads to protein conformational changes that markedly enhance catalytic activity for the conversion of guanylyl triphosphate (GTP) to cyclic guanylyl monophosphate (cGMP) plus pyrophosphate [21]. Furthermore, there have been numerous claims that NO inhibits various metallo proteins. Thus, it is of importance to characterize the dynamics and mechanisms of the reactions leading to formation (the "on" reaction) and decay (the "off" reaction) of metal nitrosyl complexes relevant to the metalloproteins, especially ferro- and ferri-heme systems. This was the context of our initial kinetics studies with Hoshino et al. [1] and subsequent investigations of the activation parameters for the "on" and "off" reactions of the water soluble ferrous and ferric complexes of water soluble porphyrinate ligands such as TPPS (tetra(4-sulfonato-phenyl)porphinato) [22] and of the ferri-heme protein met-myoglobin (metMb) [23]. Although rates of NO reactions with various iron porphyrins and heme proteins were first studied several decades ago [24], systematic mechanistic studies were relatively limited.

Since the ferri- and ferro-heme systems are relatively labile toward NO exchange, their kinetics were most effectively studied by laser flash photolysis techniques. However, in some cases, the off reactions were investigated by stopped-flow mixing of the appropriate nitrosyl complex with a NO trapping agent [23]. Photoexcitation generally results in NO labilization from Fe(Por)(L)(NO) (Por = porphyrinato dianion) followed by relaxation of the system to equilibrium (Eq. (3)). Under such conditions, the transient spectra decayed exponentially, and the observed rate constant k_{obs} could be extracted. According to this model, $k_{obs} = k_{on}[NO] + k_{off}$, and plots of k_{obs} versus [NO] were linear with slopes equal to k_{on} and intercepts equal to k_{off}. The slopes are inherently more accurate than intercepts, so k_{off} values will have a high relative uncertainty, unless the intercepts are large. It was for these latter cases that NO trapping agents were used to determine k_{off}.

$$\mathrm{Fe(Por)(L)} + \mathrm{NO} \underset{k_{off}}{\overset{k_{on}}{\rightleftharpoons}} \mathrm{Fe(Por)(L)(NO)} \qquad \mathrm{h}\nu \qquad (3)$$

Systematic measurements of k_{on} and k_{off} as functions of temperature (298–318 K) and hydrostatic pressure (0.1–250 MPa) by Laverman et al., of the water soluble Fe^{III}(TPPS) and Fe^{II}(TPPS) complexes [22] determined values of $\Delta H^{\ddagger}$, $\Delta S^{\ddagger}$ and $\Delta V^{\ddagger}$ for both processes for the former and for the "on" reactions of the latter. For the ferriheme model $Fe^{III}(TPPS)(H_2O)_2$, the large and positive $\Delta S^{\ddagger}_{on}$ and the large and positive $\Delta V^{\ddagger}_{on}$ values (Table 1) indicate a substitution mechanism dominated by ligand dissociation (Scheme 3).

If we assume that the NO substitution onto $Fe^{III}(Por)(H_2O)_2$ occurs via this dissociative mechanism, and apply the steady state approximation to the intermediate $Fe^{III}(Por)(H_2O)$, k_{obs} would be

$$k_{obs} = \frac{k_1 k_2[NO] + k_{-1}k_{-2}[H_2O]}{k_{-1}[H_2O] + k_2[NO]} \qquad (4)$$

The rapid solvent exchange process indicates that $k_{-1}[H_2O] \gg k_2[NO]$; therefore, $k_{off} = k_{-2}$ and $k_{on} = k_1k_2/k_{-1}[H_2O]$. Thus, the apparent activation enthalpy for k_{on} would be $\Delta H^{\ddagger}_{on} = \Delta H^{\ddagger}_1 = + \Delta H^{\ddagger}_2 - \Delta H^{\ddagger}_{-1}$. Differences in the activation parameters for the very fast process k_2 and the k_{-1} should be small (reactions of the unsaturated intermediate $Fe^{III}(Por)(H_2O)$ with NO and H_2O, respectively), therefore, the difference $\Delta H^{\ddagger}_2 - \Delta H^{\ddagger}_{-1}$ should also be small. Accordingly, the principal contributor to $\Delta H^{\ddagger}_{on}$ is $\Delta H^{\ddagger}_1$, the activation enthalpy for the H_2O dissociation. Similar arguments can be offered regarding $\Delta S^{\ddagger}_{on}$ or $\Delta V^{\ddagger}_{on}$, so $\Delta H^{\ddagger}_{on}$ should reflect the energy necessary to break a Fe^{III}–OH_2 bond, $\Delta S^{\ddagger}_1$ should be large and positive owing to formation of two species from one, and $\Delta V^{\ddagger}_1$ should be positive for the same reason. These conditions are met for k_{on} (Table 1). Furthermore, a recent reexamination of the exchange kinetics using variable temperature/pressure NMR gave $\Delta H^{\ddagger}_{ex}$, $\Delta S^{\ddagger}_{ex}$ and $\Delta V^{\ddagger}_{ex}$ values [25] in agreement with the k_{on} activation parameters. Thus, it is clear that the factors determining the exchange between $Fe^{III}(TPPS)(H_2O)_2$ and solvent H_2O also dominate the NO reaction with the same species.

The ferrous complex Fe^{II}(TPPS) reacts with NO about 10^3 times faster than does the ferric analog [21]. The small values of the activation parameters are consistent with rates largely defined by diffusional factors, although the k_{on} values reported are somewhat less than diffusion limits in water. High spin ferroheme proteins complexes tend to be considerably more reactive towards ligands than are ferriheme analogs and a likely explanation would be that the former are 5-coordinate or exceedingly labile.

Kinetics studies of ferro-heme proteins and model compounds have led to a suggested mechanism in which an en-

$$\mathrm{Fe^{III}(Por)(H_2O)_2} \underset{k_{-1}}{\overset{k_1}{\rightleftharpoons}} \mathrm{Fe^{III}(Por)(H_2O)} + \mathrm{H_2O}$$

$$\mathrm{Fe^{III}(Por)(H_2O)} + \mathrm{NO} \underset{k_{-2}}{\overset{k_2}{\rightleftharpoons}} \mathrm{Fe^{III}(Por)(H_2O)(NO)}$$

Scheme 3. A limiting dissociative mechanism for NO substitution onto $Fe^{III}(Por)(H_2O)_2$.

Table 1
Rate constants (k_{on} and k_{off}) and the respective activation parameters for the reactivity of NO with ferri- and ferro-heme models and proteins ($Fe(P) + NO \underset{k_{OFF}}{\overset{k_{ON}}{\rightleftharpoons}} Fe(P) + NO$)

"On" reactions[a]	k_{on} ($M^{-1}\,s^{-1}$)	$\Delta H^{\ddagger}_{on}$ ($kJ\,mol^{-1}$)	$\Delta S^{\ddagger}_{on}$ ($J\,mol^{-1}\,K^{-1}$)	$\Delta V^{\ddagger}_{on}$ ($cm^3\,mol^{-1}$)	Ref.
Fe^{III}(TPPS) + NO	4.5×10^5	69 ± 3	95 ± 10	9 ± 1	[22b]
metMb + NO	4.8×10^4	63 ± 2	55 ± 8	20 ± 6	[23]
Fe^{II}(TPPS) + NO	1.5×10^9	24 ± 3	12 ± 10	5 ± 1	[22b]
Fe^{II}(TMPS) + NO	1.0×10^9	26 ± 6	16 ± 21	2 ± 2	[22b]
"Off" reactions	k_{off} (s^{-1})	$\Delta H^{\ddagger}_{off}$ ($kJ\,mol^{-1}$)	$\Delta S^{\ddagger}_{off}$ ($J\,mol^{-1}\,K^{-1}$)	$\Delta V^{\ddagger}_{off}$ ($cm^3\,mol^{-1}$)	
Fe^{III}(TPPS)(NO)	0.5×10^3	76 ± 6	60 ± 11	18 ± 2	[22b]
metMb(NO)	42	68 ± 4	14 ± 13	18 ± 3	[23]
Fe^{II}(TPPS)(NO)	6.4×10^{-4}				[22b]

counter complex is formed prior to the ligand bond formation [24b]:

$$Fe^{II}(Por) + L \underset{k_{-D}}{\overset{k_D}{\rightleftharpoons}} \{Fe^{II}(Por)||L\} \xrightarrow{k_a} Fe^{II}(Por)L \qquad (5)$$

In this model, k_D is the rate constant for diffusion of Fe^{II}(Por) and L together, k_{-D} for diffusion apart, and k_a for the "activation" step where M–L bond formation is effected. The steady state approximation gives $k_{on} = k_D k_a/(k_{-D} + k_a)$. The limiting cases are when the reaction is diffusion limited ($k_a \gg k_{-D}$) so $k_{on} = k_D$ or when it is activation limited ($k_{-D} \gg k_a$) so $k_{on} = k_D k_a/k_{-D}$.

In the activation limited process, $\Delta V^{\ddagger}_{on} = \Delta V^{\ddagger}_{a} + \Delta V^{\ddagger}_{D} - \Delta V^{\ddagger}_{-D}$, where $\Delta V^{\ddagger}_{D} - \Delta V^{\ddagger}_{-D}$ is the small volume difference between the encounter complex and the solvent separated species. The dominant term would then be $\Delta V^{\ddagger}_{a}$, which should be negative owing to the formation of a Fe^{II}–L bond and spin state change from a quintet Fe^{II}(Por)||doublet NO encounter complex to the doublet Fe^{II}(Por)(NO). For the diffusion limited case, $\Delta V^{\ddagger}_{on} = \Delta V^{\ddagger}_{D}$, which would be positive owing to solvent viscosity increases at higher pressure [26] as was observed for Fe^{II}(TPPS) in water (Table 1).

The model described by Eq. (5) applies to analogous reactions with CO. The rate constant for the reaction of Fe^{II}(TPPS) with CO ($k_{CO} = 3.6 \times 10^7\,M^{-1}\,s^{-1}$) is several orders of magnitude below the diffusion limit [21], and, in contrast to the reaction with NO, the $\Delta V^{\ddagger}_{on}$ values for CO are negative ($-6\,cm^3\,mol^{-1}$). Thus the reaction with CO must be activation limited [27]. This model was confirmed by a study of the CO reaction with Fe^{II}(MCPH) (MCPH = monochelated protoheme, or protohemin 3-(1-imadazoyl) propylamide stearyl ester) in toluene/mineral oil solutions. Pressure effects on the solvent viscosity were used to tune the reaction mechanism from an activation limited process at low hydrostatic pressure (large negative $\Delta V^{\ddagger}_{on}$) to a diffusion limited process at higher pressures (large positive $\Delta V^{\ddagger}_{on}$) where the solvent viscosity increased dramatically [28].

4. Photochemistry of Mn(III) and Cr(III) nitrito complexes

Our initial interest in nitrito complexes was stimulated by a report from Suslick and Watson [29] that photolysis of Mn(TPP)(ONO) led to MnO–NO bond homolysis to give NO as illustrated by Eq. (6). This was reinforced by studies demonstrating that the Mo(V) and Cr(III) complexes Mo(TPP)(O)(ONO) and Cr(TPP)(ONO) undergo irreversible β-cleavage to give Mo(TPP)$(O)_2$ and Cr(TPP)(O), respectively, in benzene [30]. Such a pathway would offer an alternative "indirect" route to generating NO from a metal complex:

$$M–O–NO \rightarrow M{=}O + NO \qquad (6)$$

However, as noted above, ruthenium nitrito complexes did not demonstrate this pathway but instead led to homolysis of the metal–ONO bond to give nitrogen dioxide as the nitrogen bearing product. Similarly, when (with Hoshino) we examined the flash photolysis kinetics of Mn(TPP)(ONO) [14], the dominant photoreaction was NO_2 formation ($\Phi = 0.045$) concomitant with Mn^{II}(TPP) formation. While this result allowed us to examine the quantitative reactivities of Mn(TPP) with NO, O_2 and NO_2 (Scheme 4), it also piqued our interest

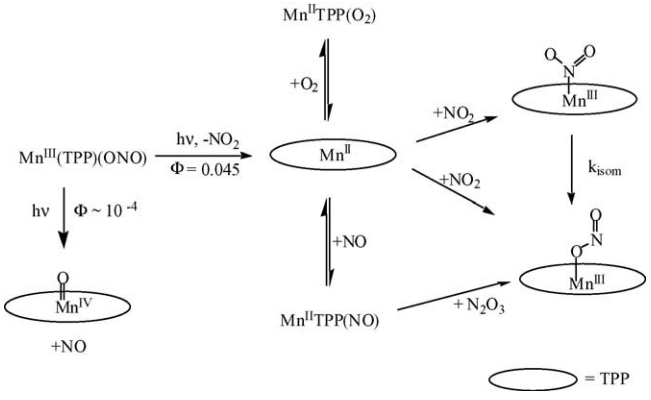

Scheme 4. Reactions of intermediates generated by flash photolysis of Mn(TPP)(ONO).

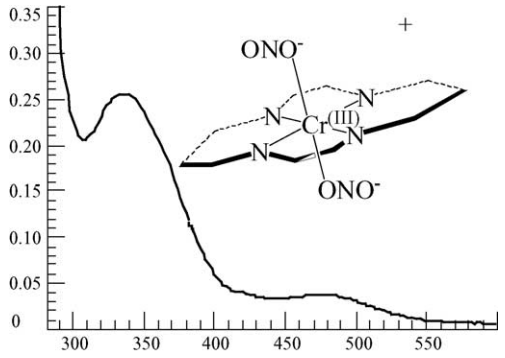

Fig. 1. Electronic spectrum of *trans*-Cr(cyclam)$(ONO)_2^+$ (cyclam = 1,4,8,11 tetraaza-cyclotetradecane) in aqueous solution.

in defining the parameters that lead to the photolytic NO generation from O-coordinated nitrite in competition with other pathways. Indeed, nitrito complexes exhibit a broad range of photoreactions including heterolysis of the M–ONO bond to labilize nitrite ion into solution as well as photoisomerization to the corresponding N-coordinated nitro complexes M–NO_2 [31].

Hoshino's results with Cr(TPPP)(ONO) clearly suggested that when nitrite is O-coordinated to an oxophilic metal, it can serve as a photochemical NO precursor. In this context, we turned to Cr(III) amine complexes to see if this behavior had generality beyond the metalloporphyrins. These are also water soluble, a desirable feature in biomedical applications. The first of such species examined was $Cr(NH_3)_5(ONO)^{2+}$, and while this was photoactive toward NO release, competing NH_3 labilization made it undesirable for comprehensive study [32].

Our attention then turned to the Cr(III) macrocyclic polyamine complex *trans*-Cr(cyclam)$(ONO)_2^+$ (cyclam = 1,4,8,11 tetraazacyclotetradecane) (Fig. 1) [33]. When this was subjected to continuous photolysis (λ_{irr} = 436 nm) in deaerated solution (or under an Ar or NO), a gradual shift of the absorption spectrum to that of the *trans*-Cr^{III}(cyclam)$(H_2O)(ONO)^+$ cation was observed. These changes were consistent with the net photoreaction under these conditions being simple photoaquation with a small quantum yield (Φ_{aq} = 0.0092), in analogy to the very low photoreactivity noted for other *trans*-Cr(cyclam)X_2^+ cations when subjected to ligand field excitation [34].

However, spectral changes were entirely different when *trans*-Cr(cyclam)$(ONO)_2^+$ was photolyzed in aerated aqueous solutions at various λ_{irr} ranging from 365 to 546 nm [32]. A new species, identified provisionally as *trans*-Cr^{IV}(cyclam)$(O)(ONO)^+$, formed and was trapped by oxygen to give a Cr(V) complex with an overall quantum yield of 0.27 at 436 nm. NO formation was confirmed electrochemically. Furthermore, flash photolysis studies indicated that the primary Cr(IV) photoproduct reacts readily with NO ($k_{NO} = 3.1 \times 10^6\ M^{-1}\ s^{-1}$) to reform *trans*-Cr(cyclam)$(ONO)_2^+$ in competition with O_2 trapping (Scheme 5). On-going studies have been concerned with modifying the ligands to introduce functional groups with strongly absorbing chromophores to serve as antennas to sensitize internally the photolysis induced NO formation as well as providing greater tissue specificity [35].

5. Iron sulfur nitrosyl clusters (Roussin's anions and esters)

5.1. Roussin's red and black salts

Although the anions of Roussin's black salt, $Fe_4S_3(NO)_7^-$ (RBS) and of Roussin's red salt, $Fe_2S_2(NO)_4^{2-}$ (RRS), were first described in the mid-19th century [36], their photochemistry has only recently drawn attention. The optical spectra of these water soluble iron/sulfur/nitrosyl clusters display strong absorptivity into the red, with moderately high extinction coefficients ($(1–3) \times 10^3\ M^{-1}\ cm^{-1}$) that suggest charge transfer character. Extended Hückel molecular orbital calculations suggest the LUMO to have Fe–Fe and Fe–S and Fe–NO antibonding character [37]; hence, excitation might be expected to lead to cluster fragmentation. However, in analogy to other Fe/S clusters [38], the metal centers may be antiferromagnetic coupled Fe^{3+} and/or Fe^{2+} with considerable ground state charge transfer to the nitrosyls. In such a case the lowest energy excited states may be NO-to-iron charge transfer states with enhanced lability of the Fe–NO bonds. There is clearly a need for a better un-

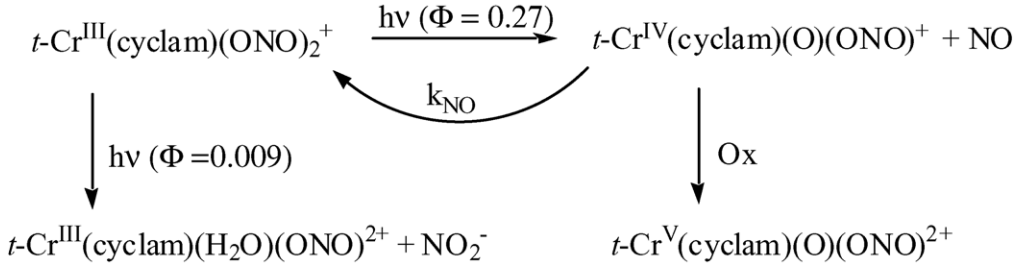

Scheme 5. Photoreaction scheme for photolysis of *trans*-Cr(cyclam)$(ONO)_2^+$ in aerated aqueous solution.

derstanding of the spectroscopy and photophysics of these clusters.

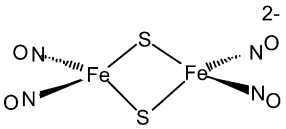

RRS

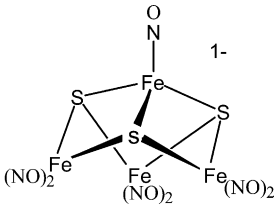

RBS

Qualitative studies demonstrated that the black salt anion serves as a photoinduced NO donor with vascular and brain tissues [39], for example rat tail artery relaxation was used to demonstrate NO release from RBS upon photolysis in buffer solutions [40]. The *quantitative* photochemistry of neither the anions nor the esters had received attention until our studies several years ago [41–44].

Photolysis of Roussin's black salt leads to optical density decreases across the visible spectrum. The quantum yields for RBS disappearance (Φ_d) showed little dependence on λ_{irr}, giving a value $\sim 10^{-3}$ from λ_{irr} 313 to 546 nm in aerated aqueous solutions [41]. However, in deoxygenated solutions, RBS showed no net photochemistry when irradiated continuously, or upon repeated laser excitation. Electrospray mass spectroscopy (ESMS), quantitative analysis for ferrous ions by 1,10 phenanthroline addition and electrochemical experiments [42] were used to identify the products photolysis in aerated aqueous solution as summarized in Eq. (7):

$$Fe_4S_3(NO)_7^- \xrightarrow[O_2]{h\nu} 3.9Fe^{2+} + 5.9NO + 3S^{2-} + ? \qquad (7)$$

Kinetic flash photolysis studies of the RBS system with time resolved optical (TRO) and time resolved infrared (TRIR) [43] spectroscopic techniques were used to probe the spectra and dynamics of possible reactive intermediates. Two transient species were formed in roughly equal concentrations, both of which are trapped by NO to reform RBS. In this context, the reaction sequence described in Scheme 6 was proposed, where X and Y are considered to be isomers of the "unsaturated cluster" $Fe_4S_3(NO)_6^-$. The combined quantum yields ($\phi_X + \phi_Y$) for formation of X and Y has a lower limit of 0.062, which can be compared to values of $<10^{-6}$, 0.0011 and 0.0042 determined in deaerated, aerated and oxygenated solutions, respectively, for the quantum yields (Φ_{RBS}) for *net* RBS decomposition according to Eq. (1) under continuous photolysis. The back reactions with NO have the second order rate constants $k_{NO}{}^x = 1.3 \times 10^7\ M^{-1}\ s^{-1}$ and $k_{NO}{}^y = 7 \times 10^5\ M^{-1}\ s^{-1}$, and it is these back reactions in competition with trapping by O_2 that determines the quantum yields for photodecomposition.

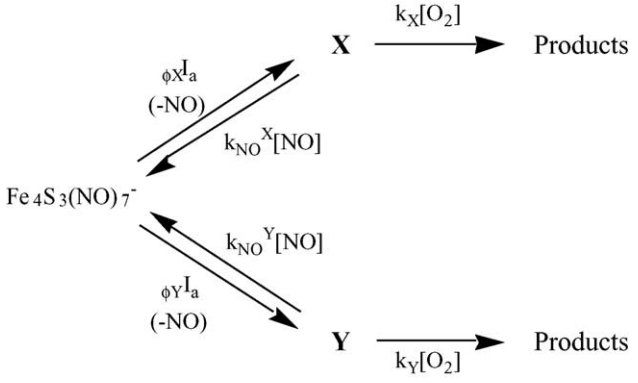

Scheme 6. Proposed reactive intermediates in flash photolysis of Roussins black salt anion.

Roussin's red salt anion is only moderately stable in aerated aqueous solutions at neutral pH, and reacts to give the more stable RBS over the course of a few hours in the dark. When irradiated with near UV or visible light, this process was markedly accelerated and gives a λ_{irr} independent quantum yield of ~0.14 for conversion of RRS [41]. However, the quantum yields are markedly dependent on the dioxygen concentration as well as the intensity of incident irradiation. This is due to the reversible reaction of primary photoproducts with NO in competition with trapping with O_2 as indicated by the flash photolysis studies described below. The RBS product was identified from optical, FT-IR and ESMS spectra: the latter also showed the formation of nitrite and sulfide. Electrochemical NO analysis indicated that 0.5 mol of NO are released for each mole of RRS converted to RBS [42].

Flash photolysis studies of $Fe_2S_2(NO)_4{}^{2-}$ demonstrated high quantum yield formation of an intermediate believed to be $Fe_2S_2(NO)_3{}^{2-}$ resulting from photodissociation of NO [43]. This species reacts competitively with NO via second order kinetics ($k_{NO} = 9.1 \times 10^8\ M^{-1}\ s^{-1}$) to reform RRS and with dioxygen ($k_{Ox} = 5.6 \times 10^7\ M^{-1}\ s^{-1}$) to give a secondary intermediate. The latter is the likely precursor of the eventual photoproduct RBS (Scheme 7). As noted above, it is this competitive trapping of the unsaturated intermediate that makes the net quantitative photochemistry strongly dependent on the O_2 concentration and the irradiation intensity.

A particularly exciting outcome of the red salt photochemical studies was the proof-of-concept demonstration in collaborative studies at the Radiation Biology Branch at the National Cancer Institute that photochemical release of NO from RRS could be used to sensitize hypoxic (oxygen deficient) cell cultures to γ-radiation damage [41]. It was clearly shown that treatment of the cells with RRS (~1 mM) alone

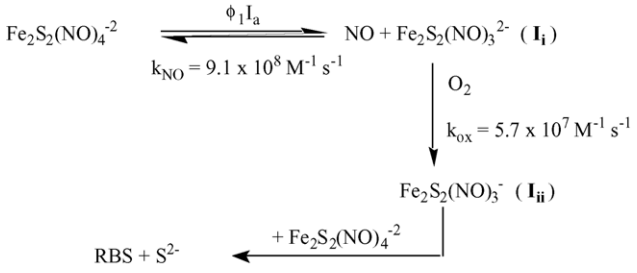

Scheme 7. Proposed reactive intermediates in flash photolysis of Roussins red salt anion.

had little effect on cell survival. Neither did visible light illumination of RRS-treated cells. However, simultaneous white light illumination of the RRS treated cell cultures enhances the killing effect of γ-radiation, and this was attributed to the sensitization of radiation induced damage by the NO photochemically released from the absorbed RRS. Sensitization effects of up to 100-fold increases in radiation induced cell death were observed for this and other red salt concentrations.

5.2. Photoreactions of the Roussin's red salt esters $Fe_2(\mu\text{-}SR)_2(NO)_4$

The red salt anions can be modified to give the so-called "red salt esters" $Fe_2(\mu\text{-}SR)_2(NO)_4$ (RSE), the syntheses of which were developed by others [45]. These can be prepared from the reaction of RRS with an alkyl halide derivative R–X (Eq. (8)) and appear to be somewhat more air stable than is RRS itself. Of particular interest is the possibility that varying the R-group will allow one to manipulate properties such as reactivity, solubility, optical spectra or biological specificity of a unit containing the iron sulfur clusters.

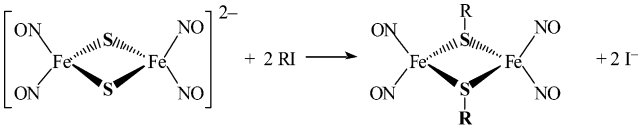

RSE

(8)

The "simple" red salt esters have characteristically similar UV–vis and IR spectra [46,47] (Fig. 2). The electronic spectra display several strong bands with maxima in the near UV. For example, the spectrum of the water soluble ester $Na_2[Fe_2(\mu\text{-}SCH_2CH_2SO_3)_2(NO)_4]$ (in which R is the β-sulfonated ethyl group) has bands with λ_{max} at 312, 364, and 430 nm, the respective extinction coefficients being 9200, 8900 and ∼4300 $M^{-1}\,cm^{-1}$. The absorption tails into the green but drops off considerably. The position and strength of these bands are relatively independent of the attached R-group (if that group is not a strong chromophore), but do show some solvento-chromism. The relatively high extinction coefficients along with the solvento-chromism suggest that they may be charge transfer in character. Because the crystal structures and spectroscopic data of the RSE compounds are similar to those of the red salt, one might assume that the sulfur substituents perturb but do not change the fundamental character of the cluster molecular orbitals.

The infrared spectra of the various red salt esters display three NO stretching bands ν_{NO}, two strong and one weak, with values that are little affected by the nature of the R-group. For R = methyl benzyl these bands appear at 1752 (s), 1774 (s) and 1808 (w) cm^{-1}. The pattern of these bands for the various esters is relatively unaffected by changing the R-substituents, but all the bands appear at higher frequency than

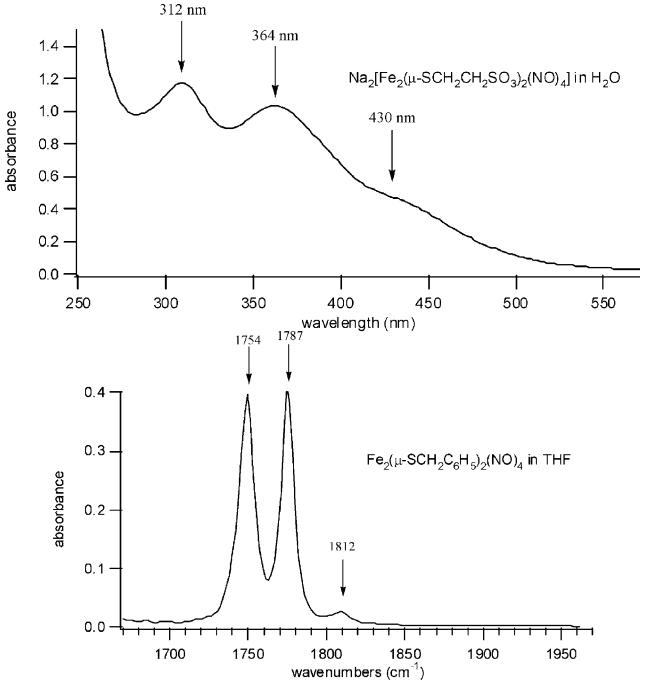

Fig. 2. Electronic and IR spectra of typical RSE. Top: electronic spectrum of $[Na_2(Fe_2(\mu\text{-}SCH_2CH_2SO_3)_2(NO)_4]$ in aqueous solution. Bottom: IR spectrum of $Fe_2(\mu\text{-}SCH_2C_6H_5)_2(NO)_4$ in THF.

the those of the red salt anion (ν_{NO}, in THF: 1653 (s), 1671 (s)), consistent with greater backbonding from the anionic Fe_2S_2 core into NO π^* orbitals in the latter case.

In the dark, solutions of the red salt esters show long term stability if deaerated but decompose slowly (over a period of few hours) under air. However, when irradiated with UV or visible light, the esters undergo photodecomposition. The specific products have not been fully characterized, although photolysis of the water soluble ester $Na_2[Fe_2(\mu\text{-}SCH_2CH_2SO_3)_2(NO)_4]$ in aerated aqueous solution was shown by using an electrochemical NO sensor to release 3.8 mol of NO per mole of ester that undergoes photoreaction. In other words, virtually all the NO is released. The other photoproducts included Fe^{2+} ions (quantitatively determined by addition of 1,10-phenanthroline) and free thiol ligands (as observed by ESMS).

The quantum yields for photodecomposition (Φ_d) (Table 2) were measured by monitoring the changes in UV–vis and/or IR absorption spectra. A broad range of values were observed depending upon the actual RSE compound and, especially, the conditions. At shorter λ_{irr} and in the presence of air, the reactions were relatively efficient (for example the photolysis of $Na_2[Fe_2(\mu\text{-}SCH_2CH_2SO_3)_2(NO)_4]$ with 365 nm light in aerated aqueous solution leads to the disappearance of the characteristic absorption spectrum of this species with a Φ_d of 0.048 ($I_a = 1.1 \times 10^{-6}$ Einstein/L s), but it is clear that the quantum yield values are dependent upon four factors: the wavelength of irradiation (λ_{irr}), the intensity of irradiation (I_0), the oxygen concentration, and the solvent.

Table 2
Quantum yields (Φ_d) for the photodecomposition of the Roussin's red salt esters (RSE) under various conditions[a] (data from Ref. [46])

Compound	Solvent	λ_{irr}[b] (nm)	I_a[c] (Einstein/L s)	Φ_d (mol/Einstein) (±~15%)
$Fe_2(\mu\text{-}SCH_3)_2(NO)_4]$	MeOH	365	3.0×10^{-6}	0.14
	CH_3CN	365	3.0×10^{-6}	0.23
	THF	365	3.0×10^{-6}	0.28
$Fe_2(\mu\text{-}SCH_2CH_3)_2(NO)_4]$	CH_3CN	365	1.1×10^{-6}	0.076
	CH_3CN[d]	365	1.1×10^{-6}	0.12
	$CHCl_3$	546	1.1×10^{-6}	1.70×10^{-4}
$Fe_2(\mu\text{-}SCH_2C_6H_5)_2(NO)_4]$	$CHCl_3$	546	1.1×10^{-6}	1.86×10^{-4}
$Fe_2(\mu\text{-}SCH_2CH_2OH)_2(NO)_4]$	MeOH	365	1.1×10^{-6}	0.079
	MeOH[d]	365	1.1×10^{-6}	0.103
	MeOH	365	3.0×10^{-6}	0.045
	MeOH	365	8.2×10^{-6}	0.002
$Na_2[Fe_2(\mu\text{-}SCH_2CH_2SO_3)_2(NO)_4]$	H_2O	365	1.1×10^{-6}	0.024
	H_2O[d]	365	1.1×10^{-6}	0.052

[a] Quantum yields for RSE loss determined from changes in UV–vis spectra. Experiments in aerated solutions at 293 K except where noted.
[b] Irradiation wavelength.
[c] Intensity of incident light.
[d] Solutions equilibrated with O_2 (1 atm).

The quantum yield response to the irradiation wavelength proved to be different from that previously observed for the photochemistry of RBS and RRS anions. This suggest that although the absorption spectra are similar to that of RRS, the excited state order may be changed in the esters to give a different, less reactive, lowest energy excited state. However, the dependence of Φ_d on the intensity of irradiation and $[O_2]$ parallel those of the anionic clusters, and again the flash photolysis studies have demonstrated that these can be explained by the primary photochemical step being the reversible labilization of NO followed by trapping of the intermediate by O_2. The solvent dependence is tied to the $[O_2]$ dependence, since dioxygen solubility varies from solvent to solvent.

Flash photolysis studies provide further insight into the aforementioned factors that influence the Φ_d values for these RSE compounds. For instance, a sample of $Fe_2(\mu\text{-}SCH_2CH_2OH)_2(NO)_4$ shows a transient bleach at 460 nm when flashed at 355 nm. Under deaerated conditions, the decay is second order and the system returns to the baseline absorbance within several hundred μs, while under air, decay is much faster and the recovery of the original absorbance is incomplete. In the latter case, the decay is roughly exponential with $k_{obs} = 2.3 \times 10^4\ s^{-1}$ giving an estimated second order rate $k_{O_2} = 1.3 \times 10^7\ M^{-1}\ s^{-1}$. A related set of flash photolysis studies were carried out with aqueous solutions of $Na_2[Fe_2(\mu\text{-}SCH_2CH_2SO_3)_2(NO)_4]$ to probe the effect of varying the NO concentration on the relaxation of the relevant intermediate. Under excess NO the transient bleach at 420 nm displayed exponential decay back to the original baseline. The resulting k_{obs} values proved to be linear in [NO], from which data a k_{NO} value of $k_{NO} = 1.1 \times 10^9\ M^{-1}\ s^{-1}$ was determined. On the basis of these studies, it was concluded that like the red salt anions (Scheme 7), the primary photoreaction of the red salt esters is the photodissociation of NO to give an unsaturated species $Fe_2(SR)_2(NO)_3$.which is competitively trapped in a very fast reaction with NO in competition with O_2 trapping and subsequent decomposition of the cluster (Scheme 8). It is evident from the photoproducts found after continuous photolysis that several other chemical transformations must occur after the trapping of the intermediate species, but these remain to be resolved.

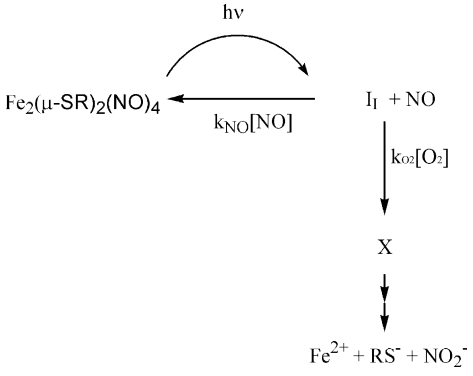

Scheme 8. Intermediates in the photolysis of RSE.

5.3. The photochemical and photophysical properties of PPIX-RSE

The similarity of the spectra of the red salt esters of the simpler R-groups to that of the red salt itself means that they also do not adsorb sufficiently at longer wavelengths for in vivo applications. To address this issue, we are preparing other RSE compounds where the R-groups have a chromophore such as a dye molecule which might act as an intramolecular photosensitizer, that is as an antenna for the $Fe_2S_2(NO)_4$ moiety. In this context, we have now prepared PPIX-RSE, a red salt ester with the R-groups being protoporphyrin-IX via the reactions shown in Scheme 9 [48]. A crystal struc-

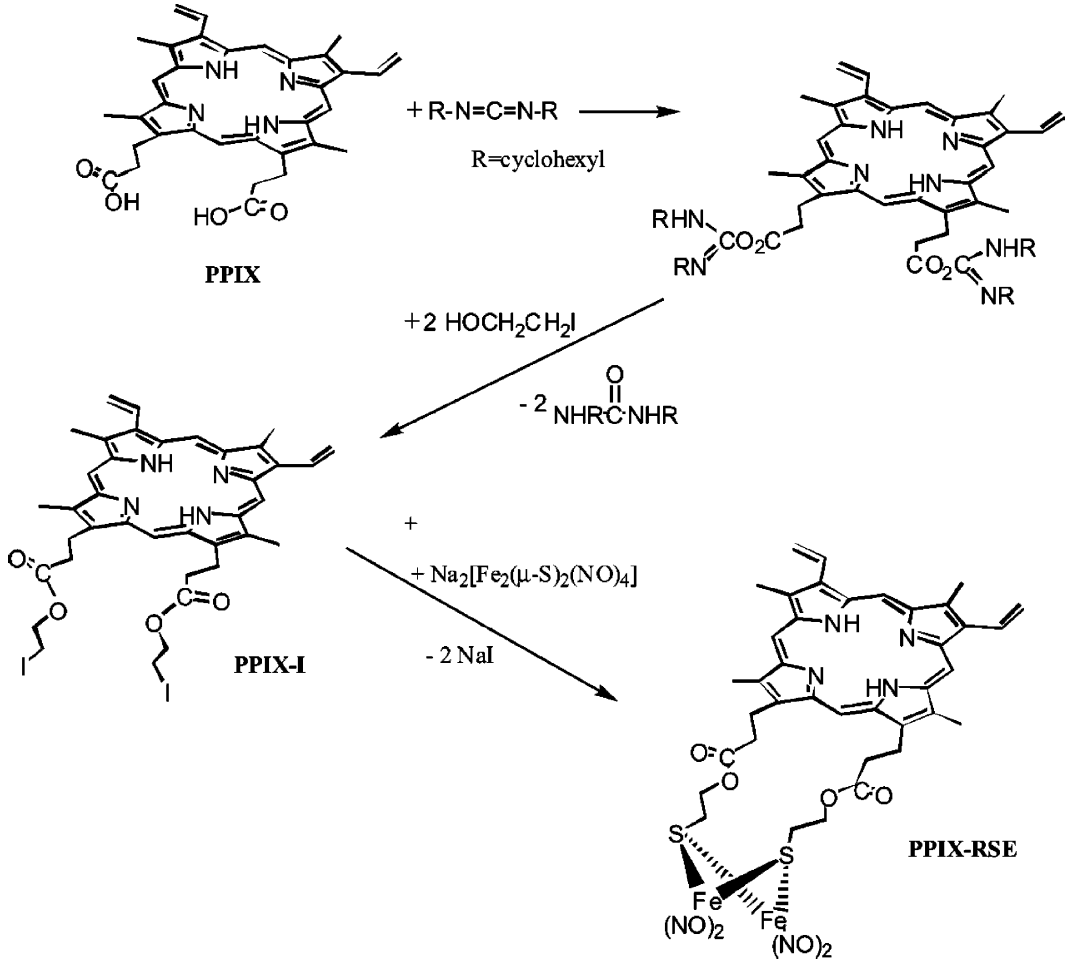

Scheme 9. Synthetic sequence to prepare PPIX-RSE.

ture has not been obtained, but a variety of physical methods including high resolution mass spectrometry and elemental analysis point to the structure depicted in Scheme 8. For example, the IR spectrum of PPIX-RSE displays the two strong ν_{NO} bands at 1754 and 1781 cm^{-1} that are characteristic of a red salt ester (Scheme 9).

The electronic spectrum of PPIX-RSE is dominated by the porphyrin chromophore with the very strong Soret band at 406 nm and the pattern of longer wavelength Q-bands (λ_{max} at ~504, 550, and 580 nm) typical of a non-metallated porphyrin (Fig. 3). However, the photophysics and photochemistry of this species are strongly influenced by the presence of the $Fe_2S_2(NO)_4$ cluster. The intensity of emission from the free base porphyrin is ~85% quenched relative to the emission from a solution containing the dimethyl ester of PPIX (DME-PPIX) or PPIX itself of the same absorbance at the excitation wavelength. Furthermore, direct excitation of the porphyrin Q-band absorptions with 546 nm light leads to NO release from the cluster with a quantum yield (2.5×10^{-4}) somewhat larger than reported for esters without the PPIX antenna (1.8×10^{-4}). This indicates intramolecular photosensitization, namely that once light is absorbed by the strongly absorbing antenna, there is energy transfer to the RRS cluster site and NO labilization as the result of the excited state generated there [48].

The steady state luminescence experiment with PPIX-RSE indicated that ~85% of the characteristic PPIX fluorescence was quenched by the presence of the RSE cluster, and this result might simply be interpreted in terms of the rate of intramolecular energy transfer being about six times the rate of radiative and non-radiative decay of the singlet state of the free PPIX chromophore.

In order to evaluate this interpretation, fluorescence lifetime measurements were undertaken [48] with Doug Magde at UC San Diego using time-correlated single-photon counting techniques [49]. Solutions of PPIX, DME-PPIX, and PPIX-RSE in THF and $CHCl_3$ were prepared such that the Soret band absorbance was between 0.6 and 0.8 in each case. Excitation was at 403 nm, and the temporal fluorescence was monitored at 632 nm. The PPIX and the DME-PPIX solutions both displayed single exponential fluorescence decay traces that could be analyzed in terms of lifetimes of 12.4 and 12.6 ns, respectively, in THF consistent with the literature [50]. However, the PPIX-RSE fluorescence decay could not be fit a single exponential, but demonstrated two lifetimes, the major component (>80% weighting) being

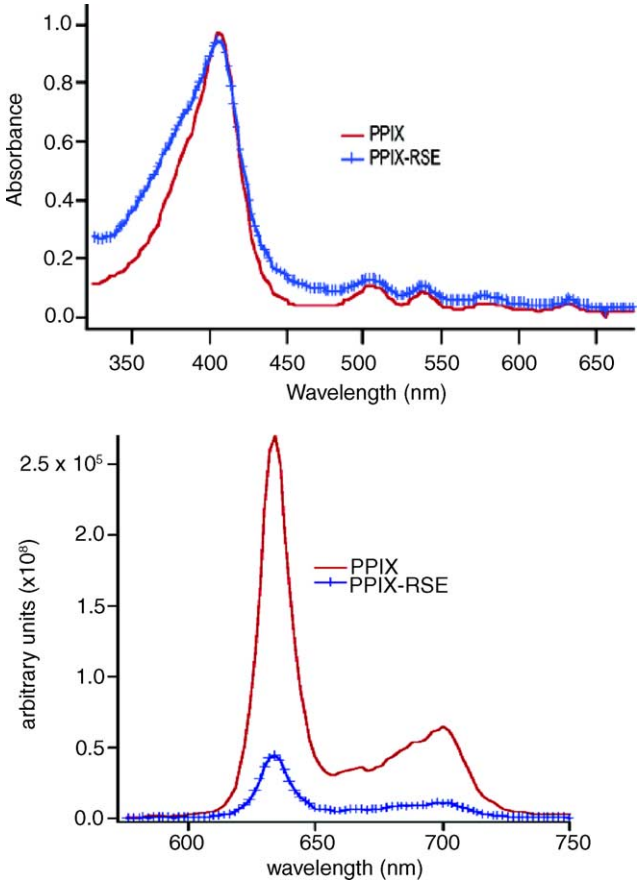

Fig. 3. Electronic spectrum and steady state fluorescence spectrum of PPIX (6.16 mM) and PPIX-RSE (6.02 mM) solutions in aerated THF at $22 \pm 0.1\,^{\circ}C$. In the electronic absorption spectrum the absorbance of the PPIX and PPIX-RSE compounds at the λ_{Soret} band (406 nm) are both equal to 0.89. The fluorescence spectra were obtained irradiating at 404 nm and monitoring the emission from 550 to 750 nm.

~200 ps, the other being similar to that of the free porphyrin at 12.6 ns.

The observation of two emission lifetimes might suggest the presence of two compounds in solution, the short lifetime being a property of PPIX-RSE and the longer one being that of a PPIX impurity. However, attempts to address this by different synthetic approaches, repeated purifications and varied spectroscopic procedures did not change the lifetimes or the weighting of the two components. Thus, we concluded that the residual emission in the steady state fluorescence measurements and the bimodal component of the emission lifetime data was truly due to the PPIX-RSE compound [48]. One might speculate that the two lifetimes might be the result of this material being present in solution in two ground state conformers, one positioned for much more efficient energy transfer from the PPIX singlet excited state to $Fe_2S_2(NO)_4$ cluster than is the other. On going studies in collaboration with the UCSB group of Michael Bowers are using a gas phase "ion chromatography" technique with time of flight mass spectroscopy [51] to examine the presence of conformers in PPIX-RSE samples.

5.4. NO release by two photon excitation (TPE) of PPIX-RSE

So far the studies reviewed here have focused on photochemical processes initiated by single photon excitation (SPE). As noted above, a desirable feature for a photo-activated drug would be responsiveness to light at longer wavelengths, for example, in the near infrared region (λ_{exc} = 800–1100 nm) where tissue penetration by light is the greatest [9]. While there are numerous chromophores that have large SPE absorption cross-sections in the UV/vis region, relatively few function in the NIR region. This led us to consider an alternative strategy where the initial excitation is generated by two-photon excitation using NIR light leading to population of higher energy states capable of exhibiting photochemistry.

The rich theory, experiments, and applications of two photon absorption (TPA) have been reviewed by others [52]. Of note is the work by Xu and Webb [53] who measured the two photon absorption cross-section (δ) of various chromophores. They also demonstrated that the fluorescence spectrum profile generated from TPA is that same as that from SPA at approximately half the wavelength. Thus both lead to formation of the same lowest energy excited state (LEES).

The two photon absorption cross-section of PPIX has been found by Goyan et al. to be $\delta_{790\,nm}$ = 2 GM [54]. TPE of free PPIX resulted in a fluorescence spectrum very similar to that generated by SPA. In this context, we investigated the photochemistry of the PPIX-RSE when subjected to TPE with NIR light [55].

In these experiments solutions of PPIX (13.5 μM), dimethyl ester-PPIX (DME-PPIX) (11.6 μM), and PPIX-RSE (13.3 μM) were prepared such that their absorbance spectra at the λ_{soret} were each nearly the same (~2). TPE fluorescence measurements were taken using a mode-locked Ti/Sapphire laser which generated 100 fs pulses with a central wavelength at 810 nm and a repetition rate of 80 MHz. The solutions were irradiated for ~3 min, and the TPE induced fluorescence was monitored from 550–750 nm. The UV–vis spectrum for both compounds and the traces for the fluorescence profiles with relative intensities are presented in Fig. 4. Notably, the UV–vis absorption spectra were are almost identical, in accordance with similar concentrations and extinction coefficients for the PPIX, DME-PPIX and PPIX-RSE compounds, respectively, but the emission behaviors of the first two differ dramatically from that of the PPIX-RSE. The emission intensity from PPIX-RSE was only ~4% that of PPIX or DME-PPIX. These observations are very consistent with the SPE steady state emission experiments at 404 nm, indicative of efficient energy transfer from the porphyrin ring to the iron sulfur cluster upon excitation of the PPIX excited state(s).

The release of NO from PPIX-RSE after TPE was demonstrated using a nitric oxide electrode sensor (an amino-700 from Innovative Instruments capable of nM NO detection

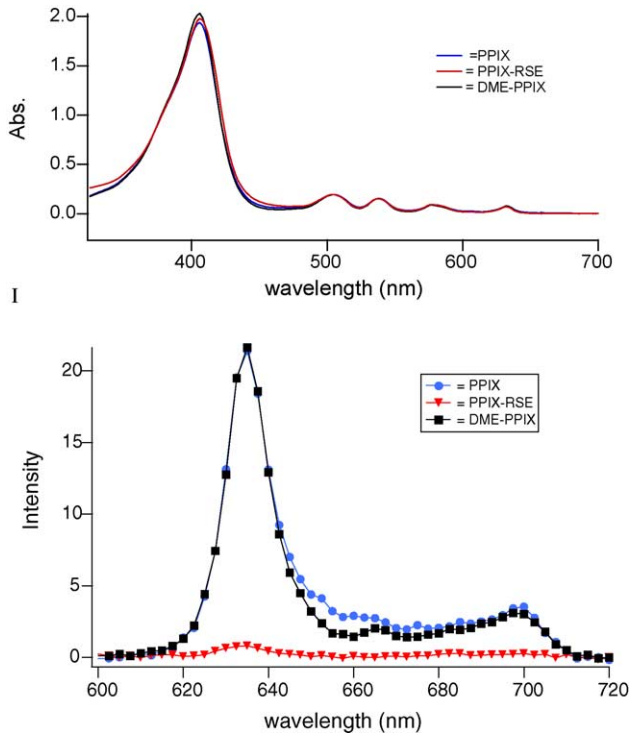

Fig. 4. Electronic spectrum and the two photon excitation (TPE) fluorescence spectrum of PPIX (13.5 μM), dimethyl ester-PPIX (DME-PPIX) (11.6 μM), and PPIX-RSE (13.3 μM) in THF at 22 °C. In the electronic absorbance spectrum the absorbance of PPIX, PPIX-DME, and PPIX-RSE compounds the λ_{Soret} band (406 nm) are all approximately 2. The fluorescence spectra were obtained by irradiating with ∼100 fs pulses at central wavelength of 810 nm and repetition rate of 80 MHz, while monitoring the emission from 550 to 750 nm.

in solution). Upon injection of the photolyzed PPIX-RSE into the NO electrode solution, immediate signal increases are observed. The first three injections were of PPIX-RSE solutions that had been illuminated with 100 fs pulses at 810 nm for 1, 1, and 3 min, respectively, and the last two injections were from PPIX-RSE solutions that had not been irradiated (these injections were done as controls to measure the amount of NO produced from thermal decomposition of the cluster) (Fig. 5). The amount of NO produced can be back calculated from the calibration curve and were found to be 2, 3, and 5 nM respectively, and ∼0 nM from the control solutions.

Further evidence for NO production was obtained via ESI+ mass spectroscopy of the solutions obtained before and after irradiation. The sole peak in the ESI + MS of the PPIX-RSE solution before irradiation was observed at *m*/*z* 913 (PPIX-RSE + H^+), but upon TPE several new peaks become apparent in the spectrum. Although some of the parent compound remains intact, a large peak at *m*/*z* 441 starts to surface in the spectrum. This peak matches nicely with the doubly charged species $[PPIX\text{-}RSE - NO]^{2+}$, and a close analysis of the peak reveals the expected isotopic pattern for a doubly charged iron species.

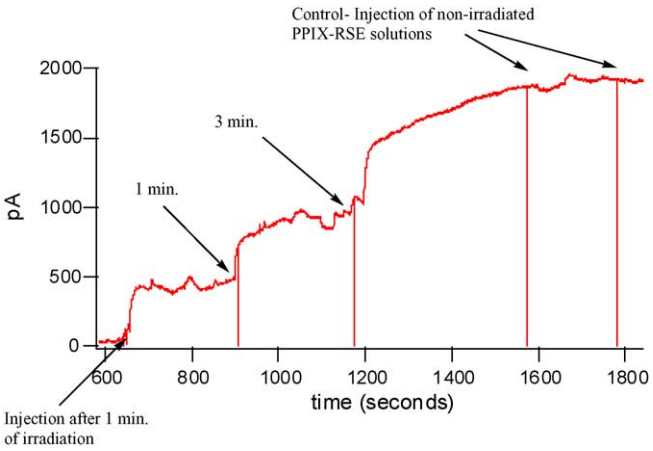

Fig. 5. Response of NO electrode to 50 μL injections of photolyzed (and nonphotolyzed control) solutions in distilled, aerated THF. PPIX-RSE solutions were irradiated from 1 to 3 min with ∼100 fs (repetition rate of 80 MHz) laser pulses and central wavelength at 810 nm.

6. Summary

This article has summarized ongoing research in this laboratory that has been concerned with the quantitative photochemistry of various metal nitrosyl compounds. The goals of these studies are two-fold: to probe the dynamics and mechanisms of the reactions of NO and NO_x species with biologically relevant model compounds and to develop new materials for the photochemical delivery of NO to specific targets. With regard to the former goal, we have examined the dynamics of NO reactions with ferri-heme proteins and models, and with regard to the latter we have described studies of ruthenium porphyrin and salen complexes, chromium(III) nitrito complexes and the iron sulfur nitrosyl clusters known as the Roussin's salts and esters. Studies of the Roussin's salts have demonstrated the concept that coordination complexes can serve as precursors for photochemical NO delivery agents to biological targets, specifically the sensitization of hypoxic cells to γ-radiation damage. Ongoing flash photolysis studies to elucidate mechanisms for the photochemical reactions of such clusters have been summarized. The ester complexes $Fe_2(SR)_2(NO)_4$ hold considerable promise as more effective delivery agents. Finally, work was discussed concerning the sensitized release of nitric oxide via both single and two photon absorption from a dye derivatized red salt ester. Further work is being pursued involving chromium cyclam, ruthenium salen and Roussin's red ester compounds which have functionalities capable of synthetic modification for the attachment of red (two photon) absorbing dyes to act as light gathering antennas at wavelengths where light transmission through tissue is more facile.

Acknowledgments

This work was supported by research grants from the U.S. National Science Foundation (CHE-0095144 and CHE-

0352650). TRO experiments were carried out on instrumentation constructed with grants from the U.S. Department of Energy University Research Instrumentation Grant Program (No. DE-FG-05-91ER79039) and from the National Science Foundation. The following students, postdoctoral fellows and visiting researchers at UCSB contributed to the studies described in this review: Katrina M. Miranda, Brian Lee, James L. Bourassa, Malcolm DeLeo, Leroy Laverman, Carmen Works, Christa Conrado, Frank DeRosa, Mark Lim, Stephen Wecksler, Dr. Setsuko Kudo and Dr. Ivan Lorkovic. Collaborations with Dr. David Wink (National Cancer Institute, Bethesda MD), Dr. Doug Magde (UC San Diego) and Dr. Mikio Hoshino (RIKEN, Japan) are also gratefully acknowledged.

References

[1] M. Hoshino, K. Ozawa, H. Seki, P.C. Ford, J. Am. Chem. Soc. 115 (1993) 9568.
[2] S. Moncada, R.M.J. Palmer, E.A. Higgs, Pharmacol. Rev. 43 (1991) 109.
[3] M. Feelish, J.S. Stamler (Eds.), Methods in Nitric Oxide Research, Wiley, Chichester, England, 1996, and references therein.
[4] (a) P.L. Feldman, O.W. Griffith, D.J. Stuehr, Chem. Eng. News 71 10 (1993) 26;
(b) D.A. Wink, I. Hanbauer, M.B. Grisham, F. Laval, R.W. Nims, J. Laval, J. Cook, R. Pacelli, J. Liebmann, M. Krishna, P.C. Ford, J.B. Mitchell, Curr. Top. Cell. Regul. 34 (1996) 159.
[5] L.J. Ignarro (Ed.), Nitric Oxide: Biology and Pathobiology, Academic Press, San Diego, 2000.
[6] F.C. Fang (Ed.), Nitric Oxide and Infection, Kluwer Academic Publishers/Plenum Press, New York, 1999.
[7] D.A. Wink, J.F. Darbyshire, R.W. Nims, J.E. Saavedra, P.C. Ford, Chem. Res. Toxicol. 6 (1993) 23.
[8] P. Howard-Flanders, Nature (London) 180 (1957) 1191.
[9] J. Mitchell, D. Wink, W. DeGraff, L. Keefer, M. Krishna, Cancer Res. 53 (1993) 5845, and references therein.
[10] (a) S. Wan, J.A. Parrish, R.R. Anderson, M. Madden, Photochem. Photobiol. 34 (1981) 679;
(b) L.O. Svaasand, R. Ellingsen, Photochem. Photobiol. 41 (1985) 73;
(c) B.R. Master, P.T. So, E. Gratton, Biophys. J. 72 (1997) 2405.
[11] K.M. Miranda, X. Bu, I. Lorkovic, P.C. Ford, Inorg. Chem. 36 (1997) 4838.
[12] L. Cheng, G.B. Richter-Addo, in: M. Kadish, K.M. Smith, R. Guilard (Eds.), The Porphyrin Handbook, vol. 4, Academic Press, New York, 2000 (Chapter 33 and references therein).
[13] I.M. Lorkovic, K.M. Miranda, B. Lee, S. Bernhard, J.R. Schoonover, P.C. Ford, J. Am. Chem. Soc. 120 (1998) 11674.
[14] M. Hoshino, Y. Nagashima, H. Seki, M. DeLeo, P.C. Ford, Inorg. Chem. 37 (1998) 2464.
[15] J.H. Enemark, R.D. Feltham, J. Am. Chem. Soc. 96 (1974) 5002.
[16] I.M. Lorkovic, P.C. Ford, Inorg. Chem. 38 (1999) 1467.
[17] (a) T. Takede, R. Irie, Y. Shinoda, T. Katsuki, Synlett 07 (1999) 1157;
(b) J. Mihara, T. Hamada, T. Takede, R. Irie, T. Katsuki, Synlett 07 (1999) 1160.
[18] C.F. Works, P.C. Ford, J. Am. Chem. Soc. 122 (2000) 7592.
[19] C.F. Works, C.J. Jocher, G.D. Bart, X. Bu, P.C. Ford, Inorg. Chem. 4 (2002) 3728.
[20] (a) J. Bordini, D.L. Hughes, J.D. Neto, C.J. Cunha, Inorg. Chem. 41 (2002) 5410;
(b) E. Tfouni, M. Krieger, B.R. McGarvey, D.W. Franco, Coord. Chem. Rev. 236 (2003) 57;
(c) M.G. Sauaia, B.G. de Lima, A.C. Tedesco, R.S. da Silva, J. Am. Chem. Soc. 125 (2003) 14718;
(d) M.G. Gomes, C.U. Davanso, S.C. Silva, L.G.F. Lopes, P. Santos, D.W. Franco, JCS Dalton (1998) 601;
(e) A.K. Patra, M.J. Rose, K.A. Murphey, M.M. Olmstead, P.K. Mascarak, Inorg. Chem. 43 (2004) 4487;
(f) E. Tfouni, J. Bordini, Private communication, from ET; A.S. Borovik, T.M. Reed, J.T. Mitchell-Koch, Angew. Chem. Int. Ed. Engl. 43 (2004) 2806.
[21] (a) A.E. Yu, S. Hu, T.G. Spiro, J.N. Burstyn, J. Am. Chem. Soc. 116 (1994) 4117;
(b) J.N. Burstyn, A.E. Yu, E.A. Dierks, B.K. Hawkins, J.H. Dawson, Biochemistry 34 (1995) 5896;
(c) G. Deinum, J.R. Stone, G.T. Babcock, M.A. Marletta, Biochemistry 35 (1996) 1540;
(d) Y. Zhao, P.E. Brandish, D.P. Ballou, M.A. Marletta, Proc. Natl. Acad. Sci. 96 (1999) 14753;
(e) M.F. Reynolds, J.N. Burstyn, in: L.J. Ignarro (Ed.), Nitric Oxide: Biology and Pathobiology, Academic Press, San Diego, 2000, Chapter 25.
[22] (a) L.E. Laverman, M. Hoshino, P.C. Ford, J. Am. Chem. Soc. 119 (1997) 12663;
(b) L.E. Laverman, P.C. Ford, J. Am. Chem. Soc. 123 (2001) [11614.
[23] L.E. Laverman, A. Wanat, J. Oszajca, G. Stochel, P.C. Ford, R. van Eldik, J. Am. Chem. Soc. 123 (2001) 285.
[24] (a) E.G. Moore, Q.H. Gibson, J. Biol. Chem. 251 (1976) 2788;
(b) E.J. Rose, B. Hoffman, J. Am. Chem. Soc. 105 (1983) 2866;
(c) M. Hoshino, S. Arai, M. Yamaji, Y. Hama, J. Phys. Chem. 90 (1986) 2109;
(d) J.W. Petrich, C. Poyart, J.L. Martin, Biochemistry 27 (1988) 4049;
(e) K.A. Jongeward, D. Magde, D.J. Taube, J. Marsters, T.G. Traylor, V.S. Sharma, J. Am. Chem. Soc. 110 (1988) 380;
(f) M. Hoshino, L. Laverman, P.C. Ford, Coord. Chem. Rev. 187 (1999) 75, and references therein.
[25] T. Schneppensieper, A. Zahl, R. van Eldik, Ang. Chemie 40 (2001) 1678.
[26] W.D. Turley, H.W. Offen, J. Phys. Chem. 88 (1984) 3605.
[27] S. Glasstone, K.J. Laidler, H. Eyring, The Theory of Rate Processes, McGraw-Hill, New York, 1941.
[28] T.G. Traylor, J. Luo, J.A. Simon, P.C. Ford, J. Am. Chem. Soc. 114 (1992) 4340.
[29] K. Suslick, R. Watson, Inorg. Chem. 30 (1991) 912.
[30] M. Yamaji, Y. Hama, M. Miyazake, M. Hoshino, Inorg. Chem. 31 (1992) 932.
[31] M.A. De Leo., P.C. Ford, Coord. Chem. Rev 208 (2000) 47.
[32] M.A. De Leo, Ph.D. Dissertation, University of California, Santa Barbara, 1998.
[33] M. De Leo, P.C. Ford, J. Am. Chem. Soc. 121 (1999) 1980.
[34] (a) C. Kutal, A.W. Adamson, Inorg. Chem. 12 (1974) 1990;
(b) N.A.P. Kane-Maguire, K.C. Wallace, D.G. Speece, Inorg. Chem. 25 (1986) 4650.
[35] F. De Rosa, Ph.D. Dissertation, University of California, Santa Barbara, 2003.
[36] F.Z. Roussin, Ann. Chim. Phys. 52 (1858) 285.
[37] S-S. Sung, C. Glidewell, A.R. Butler, R. Hoffman, Inorg. Chem. 24 (1985) 3856.
[38] L. Noodleman, E.J. Baerends, J. Am. Chem. Soc. 106 (1984) 2316.
[39] E.K. Matthews, E.D. Seaton, M.J. Forsyth, P.A. Humphrey, Brit. J. Pharmacol. 113 (1994) 87.
[40] F.W. Flitney, I.L. Megson, J.L. Thomson, G.D. Kennovin, A.R. Butler, Brit. J. Pharmacol. 117 (1996) 1549.
[41] J. Bourassa, W. DeGraff, S. Kudo, D.A. Wink, J.B. Mitchell, P.C. Ford, J. Am. Chem. Soc. 119 (1997) 2853.

[42] S. Kudo, J.L. Bourassa, S.E. Boggs, Y. Sato, P.C. Ford, Anal. Biochem. 247 (1997) 193.
[43] J. Bourassa, B. Lee, S. Bernard, J. Schoonover, P.C. Ford, Inorg. Chem. 38 (1999) 2947.
[44] J. Bourassa, P.C. Ford, Coord. Chem. Rev. 200–202 (2000) 887.
[45] (a) T.B. Rauchfuss, T.D. Weatherill, Inorg. Chem. 21 (1982) 827; (b) D. Seyferth, M.K. Gallagher, M. Cowie, Organometallics 5 (1986) 539.
[46] C.L. Conrado, J. Bourassa, C. Egler, S. Wecksler, P.C. Ford, Inorg. Chem. 42 (2003) 2288.
[47] C.L. Conrado, Ph.D. Dissertation, University of California, Santa Barbara, 2002.
[48] C. Conrado, S. Wecksler, C. Egler, D. Magde, P.C. Ford, Inorg. Chem. 43 (19) (2004) 5543.
[49] D. Magde, B.F. Campbell, SPIE 1054 (1989) 61.
[50] N.C. Maiti, S. Mazumdar, N. Periaswamy, J. Phys. Chem. 95 (1995) 10708.
[51] E.S. Baker, J. Gidden, D.P. Fee, P.R. Kemper, S.E. Anderson, M.T. Bowers, Int. J. Mass Spectrom. 227 (2003) 205.
[52] (a) B.R. Reddy, Crit. Rev. Opt. Sci. Technol. (2000) 87; (b) K. Konig, J. Microsc. 200 (2000) 83; (c) P.R. Callis, Ann. Rev. Phys. Chem. 48 (1997) 271; (d) P.N. Prasad, D.J. Williams, Introduction to Non-linear Optical Effects in Molecules and Polymers, Wiley, New York, 1991; (e) Y.R. Shen, The Principles of Non-linear Optics, Wiley, New York, 1984.
[53] C. Xu, W.W. Webb, J. Opt. Soc. Am. B 13 (1996) 481.
[54] R.L. Goyan, D.T. Cramb, Photochem. Photobiol. 72 (2000) 821.
[55] S. Wecksler, A. Mikhailovsky, P.C. Ford, J. Am. Chem. Soc. 126 (2004) 13566.